Aerospace Science and Technology 45 (2015) 398–407

Contents lists available at ScienceDirect

Aerospace Science and Technology

www.elsevier.com/locate/aescte

High altitude propeller design and analysis

J. Morgado [a,*], M. Abdollahzadeh [b], M.A.R. Silvestre [a], J.C. Páscoa [b]

[a] University of Beira Interior, Aerospace Sciences Department, Edifício II das Engenharias, Calçada Fonte do Lameiro, no. 1, 6201-001 Covilhã, Portugal
[b] University of Beira Interior, Electromechanics Department, Edifício I das Engenharias, Calçada Fonte do Lameiro, no. 1, 6201-001 Covilhã, Portugal

ARTICLE INFO

Article history:
Received 17 December 2014
Received in revised form 7 June 2015
Accepted 9 June 2015
Available online 12 June 2015

Keywords:
JBLADE
Propeller inverse design
Propeller analysis
High altitude propeller
CFD propeller simulation

ABSTRACT

This paper presents the design and optimization of a new propeller to use on the MAAT cruiser airship. The inverse design methodology is based on minimum induced losses and was implemented in JBLADE software in order to obtain optimized geometries. In addition, the design procedure and the optimization steps of a new propeller to use at high altitudes are also described. The results of propellers designed with JBLADE are then analyzed and compared with conventional CFD results, since there is no experimental data for these particular geometries. Two different approaches were used to obtain the final geometries of the propellers. Instead of using the traditional lift coefficient prescription along the blade, the airfoil best $L^{3/2}/D$ and best L/D were used to produce different geometries. It is shown that this new design approach allows the minimization of the chord along the blade, while the thrust is maximized.

1. Introduction

The airships appeared in the end of 19th century and the first air transportation services were run by these controlled lighter-than-air vehicles. After a promising development in the beginning of 20th century, the crash of *LZ 129 Hindenburg* in May of 1937, led to the end of operations of the commercial airship transportation service and, thereafter, to almost 60 years of inactivity. Recently, the rapid progress of aerospace technologies [1,2], brought the airships back as a new platforms for undertaking multiple tasks [3]. In particular, stratospheric airships have been considered as an excellent platform for many different purposes such as aerial exploration, surveillance and monitoring or even as a solution for aerial transportation [4–9].

Multibody Concept for Advanced Airship for Transport (MAAT [10–12]) project is a collaborative European project which aims to develop a heavy lift cruiser-feeder airship system in order to provide middle and long range transport for passengers and goods. The MAAT airship will be composed by 3 different main modules: Airship Hub Airport (AHA) – located in the important logistic and near cities centers, where the airships will perform ground operations; Air Transport Efficient Network (ATEN) – feeder – an airship with its vertical take-off and landing capabilities used as connection between the ground and the cruiser; Photovoltaic Transport Airship for High-altitudes (PTAH) – cruiser – an airship to carry the cargo or passengers delivered by different feeders which remains airborne on stable routes on higher altitudes than civil aviation routes [11].

Propellers have been used as propulsion units in different types of aerial vehicles, including airships. In order to obtain an efficient propeller it is essential to have a reliable numerical tool to model its propulsive performance. The propeller optimization process can start from an inverse design method which gives us the blade geometric characteristics for a pre-determined operating point. This base blade geometry can then be used for a parametric/sensitivity analysis to judge its relative merit in the overall flight envelope.

The design of the propeller based on minimum induced losses started with Betz [13] and Goldstein [14] in the beginning of the 20th century. In 1936 Glauert [15] used the equations provided by Betz but without any organized procedure for designing the propellers. Also during 1936, Bierman [16] developed one of the first parametric studies, analyzing the influence of some parameters during propeller design. He analyzed the reduction in the design pitch angle in function of the propeller operating speed and the thrust and/or power increase. Theodorsen [17] showed that the Betz condition for minimum energy loss can also be applied for heavy disk loadings. Later in 1979, Larrabee [18] reviewed Glauert's work to produce a straightforward process to produce new propeller geometries. However, the method still has some problems: small angle of attack approximation, low disk loadings and does not include viscous terms in the induced velocity formulation. During 1990, Theodorsen's developments were later revisited by Riber and Foster [19]. Recently in 1994 Adkins and Liebeck [20] presented some improvements on the previous work bringing a new design method, without small angle of attack approximation

* Corresponding author. Tel.: +351 96 748 06 76.
E-mail address: jmorgado@ubi.pt (J. Morgado).

http://dx.doi.org/10.1016/j.ast.2015.06.011
1270-9638/

Nomenclature

a_a	Axial induction factor	R	Propeller tip radius ..... m
a_t	Tangential induction factor	Re	Reynolds number
B	Number of blades	T/A	Disk loading ..... N/m^2
C_D	Airfoil drag coefficient	V	Freestream velocity ..... m/s
C_f	Skin friction coefficient	x	Non-dimensional distance, $\Omega r/V$
C_L	Airfoil lift coefficient	y^+	Non-dimensional wall distance
C_p	Power coefficient	α	Angle of attack
C_t	Thrust coefficient	ε	Drag-to-lift ratio
Eta	Propeller efficiency	ζ	Displacement velocity ratio, v'/V
F	Prandtl's factor	θ	Incidence angle
G	Circulation function	λ	Speed ratio, $V/\Omega R$
L/D	Lift to drag ratio	ξ	Non-dimensional radius, r/R
M	Mach number	ϕ	Inflow angle
r	Radius of blade element position ..... m	ϕ_t	Tip inflow angle

Table 1
High-altitude propeller data.

Year	Aircraft name	Propeller thrust, N	Propeller diameter, m	T/A, N/m^2
1987	Egrett [21,22]	2773	3.04	305.42
1988	Condor [23]	1129	4.90	59.87
1993	Pathfinder [23,24]	23	2.01	7.25
1994	Perseus [25]	388	4.40	102.07
1995	Strato 2C [26]	2500	6.00	88.42
1996	Theseus [27]	409	2.74	69.36

and some of the light disk loading limitations, which better agrees with the analysis of the designed propeller.

Design and optimization of a high altitude propeller can be a challenging problem due to the extremely low air density. Even so, propellers are being used in many high altitude aircrafts such as: Egrett (1987) [21,22], Condor (1988) [23], Pathfinder (1993) [23,24], Perseus A (1993), Perseus B (1994) [25], Strato 2C (1995) [26], Theseus (1997) [27], Pathfinder Plus (1998), Centurion (1998) and Helios (1999). Although there is only little information about high altitude propeller design, a summary of the propellers characteristics is given in Table 1.

2. Methodology

2.1. JBLADE overview

JBLADE [28–32] is a numerical open-source propeller design and analysis software written in the C++/QML programming language [33]. The code is based on QBLADE [34,35] and XFLR5 [36] codes. It can estimate the performance of a given propeller geometry for off-design analysis and has a graphical interface making easier to build and analyze the propeller simulations.

With the coupling between a BEM formulation module and XFOIL [37], the airfoil characteristics needed for the blades simulation can be obtained through a direct analysis of each airfoil. The coupling between these modules allows the design of airfoils and the computation of their lift and drag polars. Furthermore, in order to improve the accuracy of the propeller analysis, the software allows the integration of airfoil data from experiments.

The simulation procedure starts by importing the blade's sections airfoils coordinates into the XFOIL module. An analysis of the performance for each airfoil over the largest possible angle of attack range is then executed. To ensure good accuracy in the propeller simulation results it is important to define the blade operational Reynolds and Mach numbers within XFOIL. Therefore, some iterations may be needed for a complete propeller simulation. These XFOIL airfoil performance polars are used to obtain a full 360° range of angle of attack airfoil polar. This polar extrapolation calculates the lift and drag coefficients of each airfoil for the complete range of angle of attack, removing any blade twist angle limitations.

The introduction of the blade geometry is made by specifying an arbitrary number of sections characterized by their radial position, chord, twist, length, airfoil and its associated *360°* angle of attack range lift and drag polar. The propeller number of blades and hub radius must be specified as well.

The propeller performance results, which characterize the propeller, are then calculated and stored. It is possible to define different simulations for the same propeller, making easy to perform parametric studies. The density viscosity and speed of sound of the fluid can be modified according to the altitude in which the propeller will operate.

2.2. Propeller inverse design in JBLADE

Although the detailed description of the inverse design method can be found in Adkins and Liebeck [20] paper, a brief description of the method is given herein. To initiate the design, the user should specify the number of blades, the hub radius and define the position and airfoil of each section of the blade. The number of sections and their location can be arbitrarily chosen. Furthermore, to obtain an initial geometry of the propeller, the free stream speed, air density and the power that the propeller absorbs or the thrust that it needs to produce must be given. The implemented method requires the equivalence between momentum equations and circulation equations which results in the relation between ζ and the induction factors as presented in Eqs. (1) and (2):

$$a_a = \frac{\zeta}{2}\cos^2\phi(1-\varepsilon\tan\phi) \tag{1}$$

$$a_t = \frac{\zeta}{2x}\sin\phi\cos\phi\left(1+\frac{\varepsilon}{\tan\phi}\right) \tag{2}$$

After the determination of the drag-to-lift ratio and angle of attack for each station, the blade chord and blade twist angle are computed as presented in Eqs. (3) and (4) respectively:

$$c = \frac{4\pi\lambda G V R\zeta/C_L B}{V(1+a_a)/\sin\phi} \tag{3}$$

$$\theta = \alpha + \phi \tag{4}$$

The four derivatives of I and J should be calculated and integrated along the radius in order to calculate the new ζ. Since the updated ζ is calculated, it is necessary to compare it with the previously calculated value to check for convergence. If it is not the case, the

Table 2
Atmosphere conditions for an altitude of 16 000 m.

Designation		Units
Air density	0.165	kg/m^3
Absolute viscosity	1.44×10^{-5}	kg/(m s)
Speed of sound	295.07	m/s

Table 3
Initial considerations for the study of number of propellers.

Designation		Units
Total thrust	339 650	N
Disk loading	300	N/m^2
Total area of actuator disk	1132.17	m^2

procedure needs to be repeated. The method takes into account the tip losses, according to Prandtl's formulation, as presented in Eqs. (5) and (6).

$$F = \frac{2}{\pi}\cos^{-1}\left(e^{-f}\right) \tag{5}$$

$$f = \left(\frac{B}{2}\right)\frac{1-\xi}{\sin\phi_t} \tag{6}$$

The inflow angle is calculated using ζ and the tip's inflow angle, as presented in Eqs. (7) and (8)

$$\tan\phi = \frac{\tan\phi_t}{\xi} \tag{7}$$

$$\tan\phi_t = \lambda\left(1 + \frac{\zeta}{2}\right) \tag{8}$$

2.3. Propeller design procedure

The main goal of the propeller is to transfer the power supplied to its shaft to the axial acceleration of the air stream as efficiently as possible. Propellers operating at high altitudes experience a number of unique design issues that must be addressed, namely the low dynamic pressure acting on the blades due to low air density and limited tip speed for reasonably low compressibility losses. The changes in the atmospheric conditions with altitude are herein assumed to correspond to the International Standard Atmosphere (ISA) [38]. The main properties of the atmosphere in which the propeller will operate are presented at Table 2.

The total thrust needed for the MAAT airship, which will be used as an input parameter for the propeller design is presented in Table 3. The disk loading was initially selected based on the data analysis of Table 1. After selecting the 305.42 N/m^2 as the disk loading, an initial study on the number of propellers needed to reach the total thrust was performed.

The implemented parametric study (see Fig. 1) shows that if 50 propellers are selected, each one needs to provide 6.79 kN of thrust. After some iteration between the inverse design method and the off-design analysis, it was decided to increase the diameter to 6 m, which had reduced the disk loading to around 240 N/m^2 (see Table 4). The rotation speed was computed using a fixed Mach number of 0.6 at the blade's tip.

2.3.1. Airfoil development

Since the L/D ratios are required as an input for the inverse design methodology, different airfoils were analyzed with the XFOIL module at the operating Reynolds and Mach numbers enabling an initial look at the airfoil characteristics. The L/D ratio has a small but noticeable effect on the final blade chord and twist and a significant effect on the propeller performance.

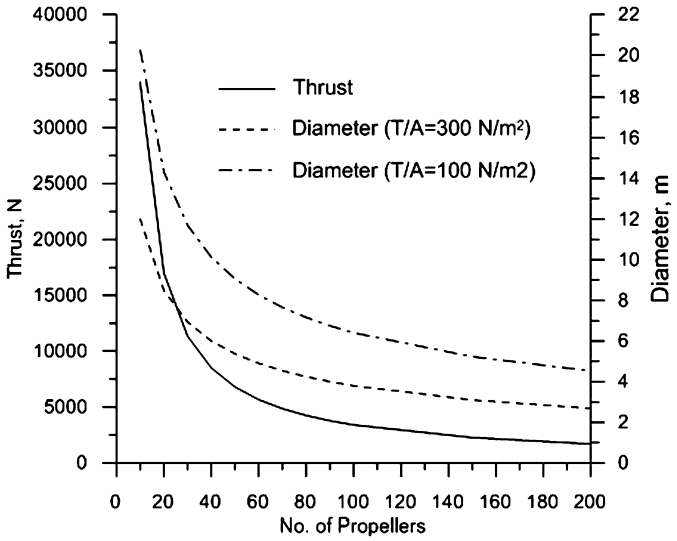

Fig. 1. Parametric study of the number of the propellers.

Table 4
MAAT cruiser propulsion.

Designation		Units
No. of propellers	50	
Propeller thrust	6.79×10^3	N
Rotation speed	550	rpm
Propeller diameter	6	m
Disk loading	240.15	N/m^2

The airfoil with highest $L^{3/2}/D$ from those that were analyzed (see Fig. 2) was then set as a base airfoil and improved [39] for a Reynolds number of 5.00×10^5. Thus, the airfoil's L/D within a useful angle of attack range was improved, allowing a reduction of the power required by the propeller for the selected disk loading and thrust. Since we are working at high altitudes, the blade chord calculated through the inverse design methodology tends to be large, leading to propellers with high solidity.

The comparison between the base and the improved airfoils shape and their pressure coefficient distribution along the chord are presented in Fig. 3. Their polars are presented in Fig. 4. It is possible to observe that the improved airfoil presents higher $L^{3/2}/D$ and L/D ratios and at the same time, these maxima ratios occur for higher lift coefficients, leading to a reduction of the blade chord needed to generate a given thrust.

2.3.2. Propeller geometry

A propeller operating design point consists of the airship's velocity, the thrust that the propeller needs to produce, the propeller hub and tip radius, the position of each intermediate section and the air properties at the desired altitude. The Reynolds number at $r/R = 0.75$ is then estimated for the selected operating point (see Tables 2 and 3). This was used to calculate the airfoil aerodynamic characteristics. The airfoil data were extrapolated and became available for full 360° angle of attack range. These data were then used by the inverse design sub-module of JBLADE, allowing the calculation of an optimal blade geometry.

A new approach for the propeller design was used herein. Instead of using a prescribed lift coefficient distribution, the software allows usage of the airfoil's best $L^{3/2}/D$ or best L/D for all sections, which leads to the minimization of the needed chord along the propeller's blade. Similarly, to some cases described in the literature [23,40] the same airfoil was used from root to tip. In the future, airfoils can be optimized for the respective position, which will allow even further improvement of the overall propeller

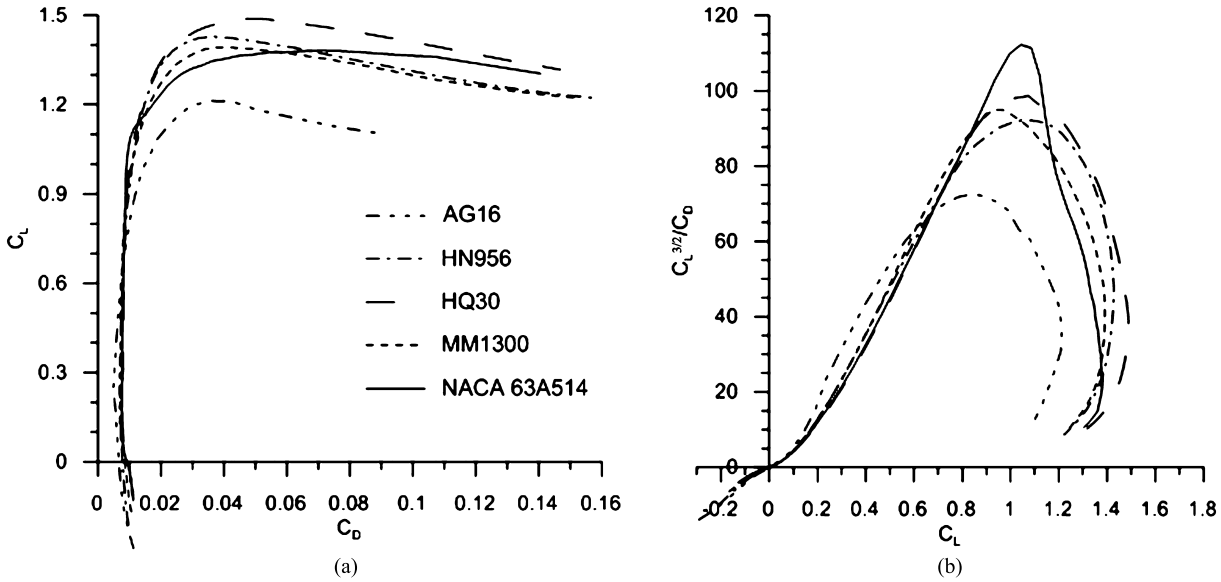

Fig. 2. Airfoils comparison performed in JBLADE's XFOIL sub-module for $Re = 5.00 \times 10^5$ and $M = 0.1$. (a) C_L vs C_D, (b) $C_L^{3/2}/C_D$ vs C_L.

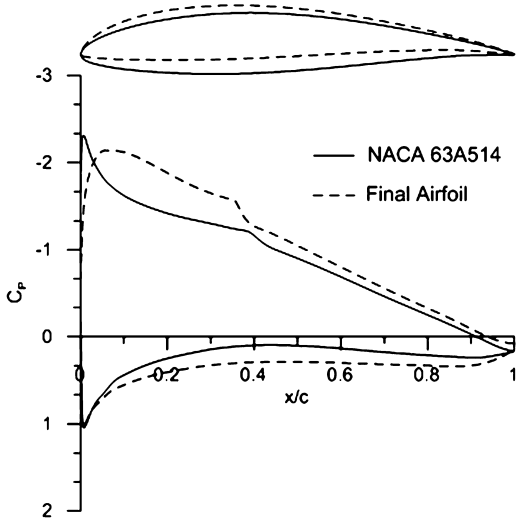

Fig. 3. Pressure coefficient distributions obtained with JBLADE's XFOIL sub-module for $Re = 5.70 \times 10^5$, $M = 0.41$ and $\alpha = 6.0°$.

performance. Since JBLADE does not contain any formulation to account with the sweep of the blades, the quarter chord of the airfoil was maintained coincident with the axis.

After obtaining the initial geometry, the off-design propeller performance was computed and the Reynolds and Mach numbers distributions along the blade radius were determined (see Fig. 5). The airfoil polars along the blade were updated for these actual Reynolds and Mach distributions and the inverse design methodology was applied again. This procedure was repeated until no evolution was observed in the blade's chord and twist.

Two different propellers were designed following the above described design procedure. One used the airfoil best L/D and the other was developed using the airfoil best $L^{3/2}/D$. These geometries are compared in Fig. 6. For both designs, the hub radius was fixed at 0.2 m and the tip radius was set to 3 m. The improved airfoil presented in Figs. 3 and 4 was used in the propellers blades.

2.4. Computational fluid dynamics

Since there is no experimental data for the presented blade, numerical simulations of the actual flow were performed to compare with the JBLADE software simulations. The computational fluid dynamics simulations were used to study the features of the flow structure and to obtain more detailed information such as parameters that affect the flow and the efficiency of the propeller.

The used airfoil was exported from JBLADE and imported in the CAD software with the respective chord and twist distribution along the blade radius. Each section was translated making the *xx* axis coincident with the 25% of the chord. The airfoils were then rotated for the respective section twist according to Fig. 6(a) and a multi-section body was built.

2.4.1. Mesh generation and boundary conditions definition

The computational domain was composed of about 2.7 million tetrahedral cells clustered around the blade surface as presented in Fig. 7. The boundaries of the domain representing the free stream conditions were set at 3 radius to the inlet and 10 radius to the outlet (see Fig. 7).

The blade (see Fig. 8) was defined by 300 nodes on the spanwise and 200 nodes on the chordwise direction.

Mesh independency tests were performed (see Fig. 9) to ensure that the obtained results are not dependent on the used mesh. As presented in Fig. 9, three different grids were used to ensure the results independency. The coarse mesh was composed by 1.65 million cells, the used mesh was made by 2.7 million and the refined mesh consisted in 4.18 million cells. The maximum discrepancy between the used mesh and the refined mesh was 3.9% for thrust coefficient and 4.2% for the power coefficient. Thus, since the result is not affected and in order to save computational time the mesh with 2.7 million was used in the remaining calculations. Furthermore, in order to reduce the computation time and facilitate the meshing process, periodic boundary conditions were also used. The y^+ was controlled by the external refinement of the mesh near the blade, through the creation of prismatic cells around the surface of the blade such that the first point above the blade surface had a value $y^+ < 1$. As presented in Fig. 7, the inlet, the outlet and the far domain were defined with a pressure far field boundary condition. At these boundaries the flow speed and direction are prescribed by inputting the value of the Mach number and the direction of the flow along the domain, together with the values of static pressure and temperature.

The values of the pressure and temperature were set according to ISA model to correspond to an altitude of 16 000 m above

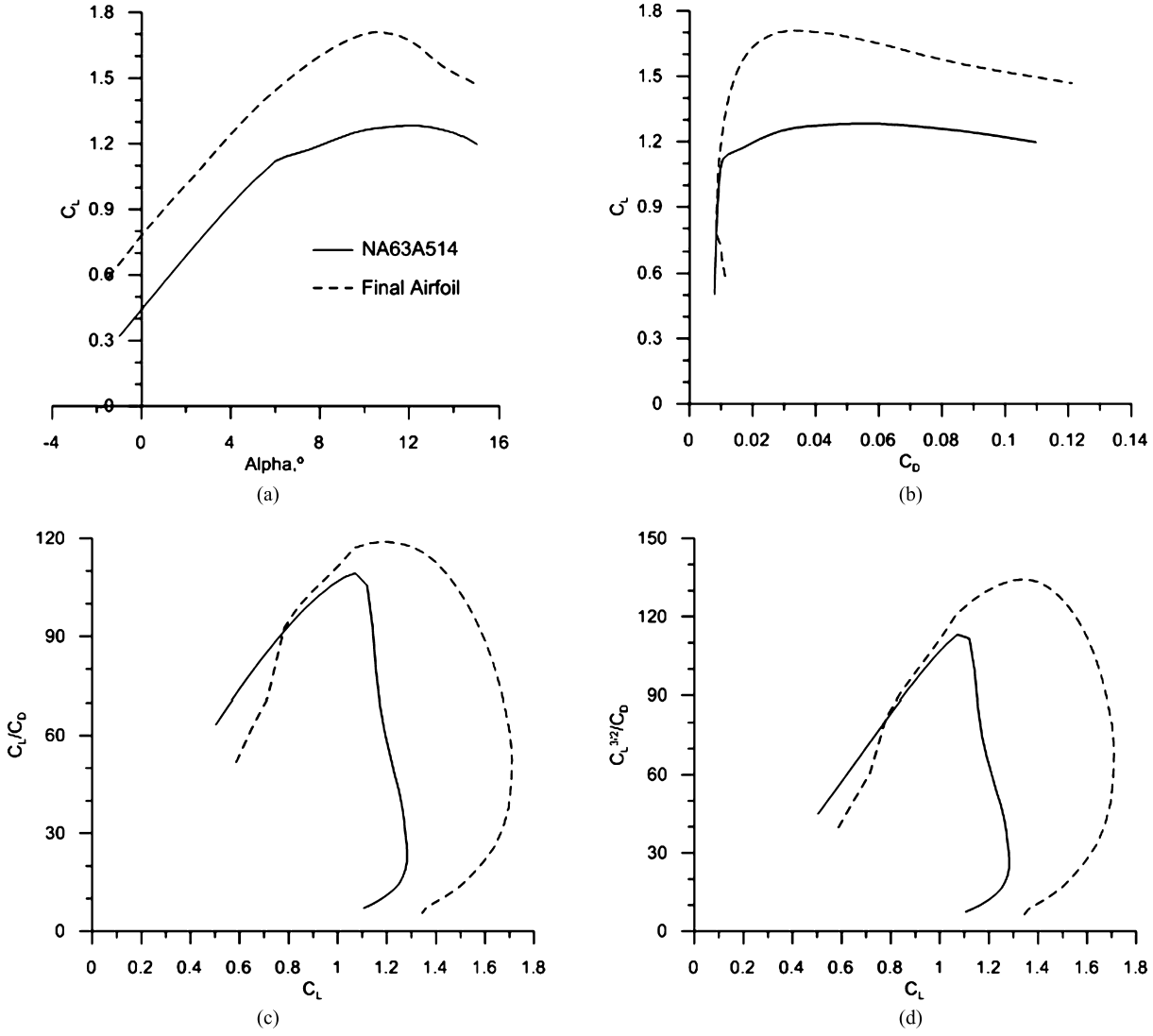

Fig. 4. Comparison between base and final airfoils for $Re = 5.70 \times 10^5$. (a) C_L vs α, (b) C_L vs C_D, (c) C_L/C_D vs C_L, (d) $C_L^{3/2}/C_D$ vs C_L.

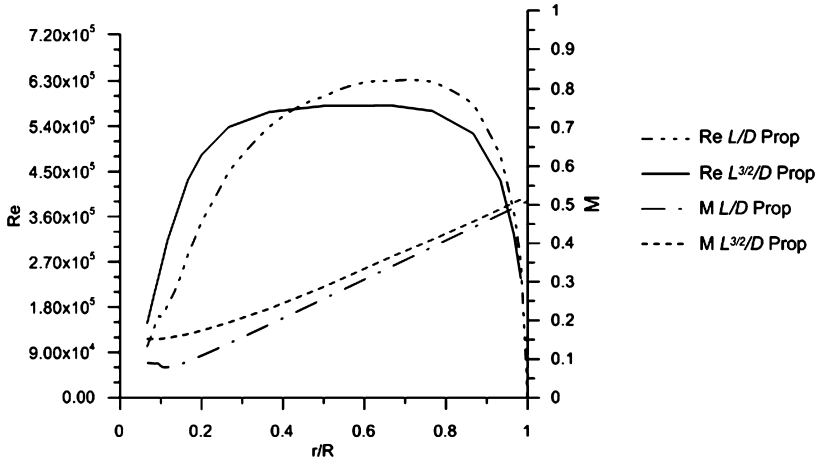

Fig. 5. Final Reynolds and Mach numbers distribution along the blades for $V = 28$ m/s.

mean sea level. The value of turbulent intensity and viscosity ratio assigned to these boundaries were 0.1% and 10 respectively. The blade surface was defined as a wall with no slip by considering the blade as a stationary wall with respect to the adjacent zone.

2.4.2. Numerical simulation procedure

Numerical simulation of steady compressible Reynolds-Averaged Navier–Stokes (RANS) equations and the turbulent mode with absolute velocity formulation was accomplished by discretizing the governing equations according the finite volume method (FVM) us-

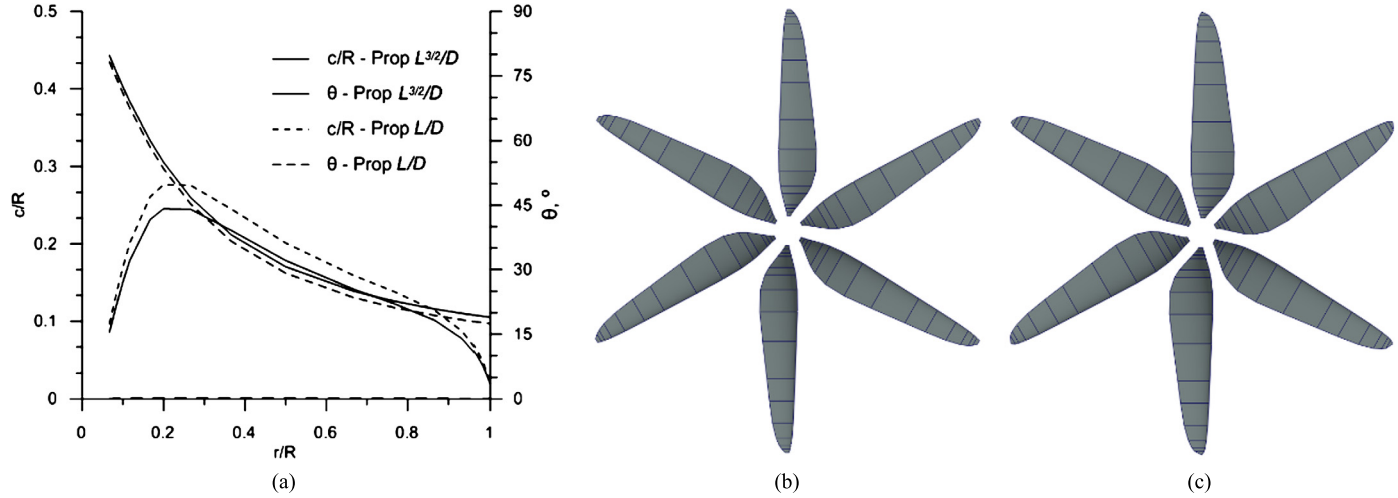

Fig. 6. (a) Comparison of propellers geometries, (b) $L^{3/2}/D$ propeller, (c) L/D propeller.

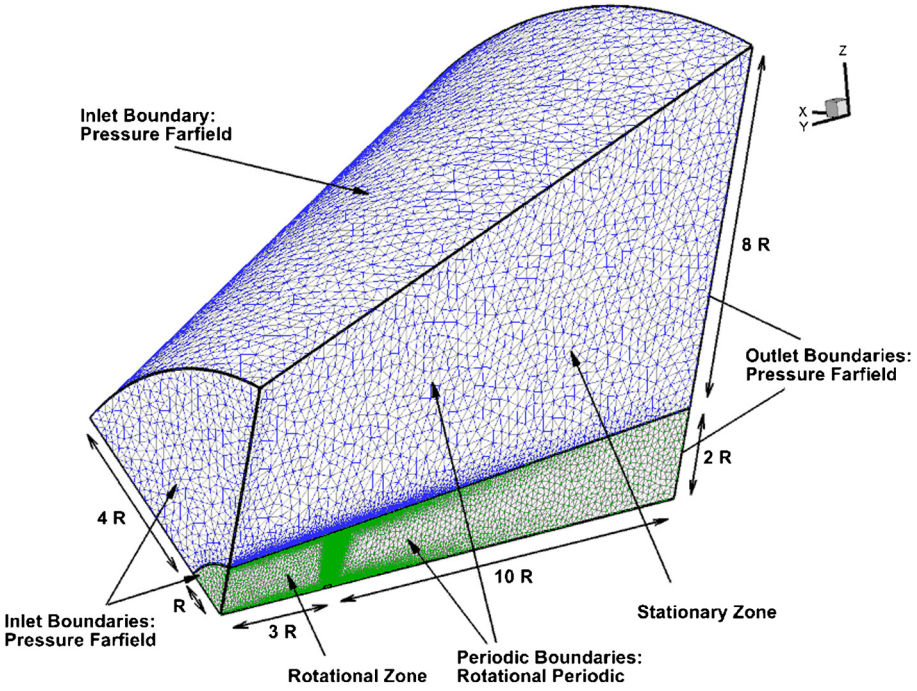

Fig. 7. Representation of the computational domain and its boundary conditions.

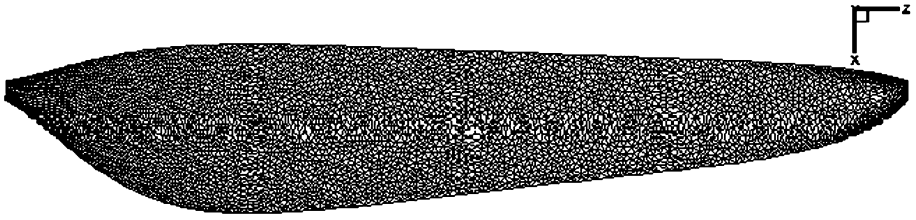

Fig. 8. Distribution of the cells on the blade surface.

ing a cell centered collocated arrangement of primitive variables. Moreover k–ω *SST* turbulence model [41] was used to deal with the time-averaging of the flow equations for simulating the turbulence.

The domain was divided in two regions: the rotating and stationary zones as presented in Fig. 7. The Multiple Reference Frame (MRF) method was chosen to accomplish the blade rotation, preventing the need to perform transient calculations by solving the governing equations in rotational reference frame considering the centrifugal and Coriolis acceleration. This method is better suited for steady state simulations where the unsteadiness of the problem can be ignored. Furthermore, the implicit coupled density based solver available in ANSYS Fluent® was selected for the coupling between momentum and continuity equations. Spatial discretization of the flow convective fluxes and turbulence variables was performed by high order advection upstream splitting method (AUSM)

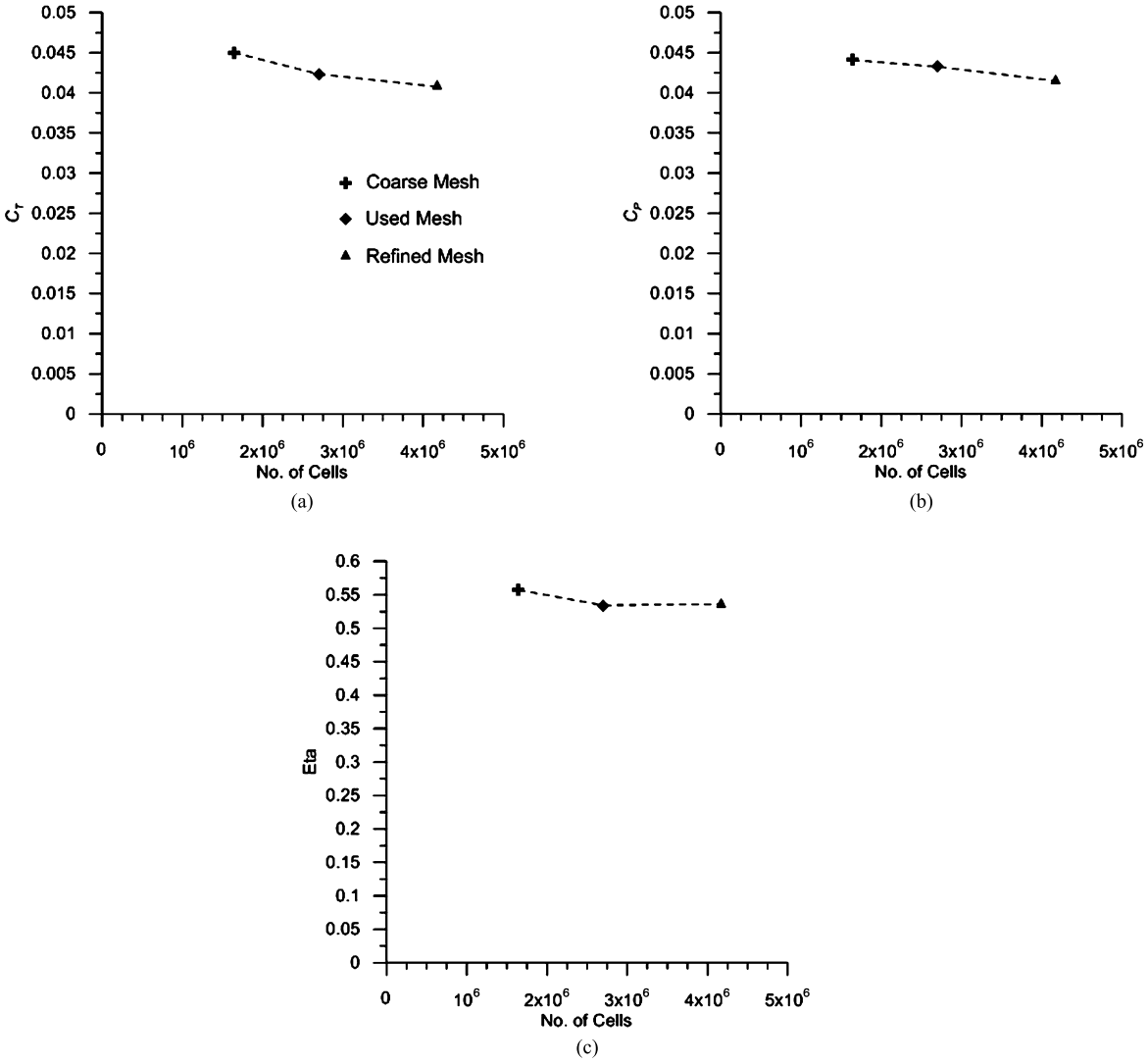

Fig. 9. Mesh independency study made for $L^{3/2}/D$ propeller at $V = 30$ m/s. (a) Thrust coefficient, (b) power coefficient, (c) propeller efficiency.

schemes and second order upwind scheme respectively. Moreover, least square cell based method was used for all the gradients. The CFD solution corresponds to a rotating domain speed of 550 rpm. To facilitate the convergence of the solution during the simulation, the rotational speed was increased gradually from 100 rpm to the final rotational speed of 550 rpm. The convergence of the numerical solution is controlled by assigning 1 to the Courant number for the iterative solution and considering suitable under relaxation factors for the turbulent variables. The convergence of the solution is also guaranteed by monitoring the relative numerical error of the solution drop below 1.0×10^{-7}. In order to compare the results of the numerical simulation with the obtained results from the JBLADE software, the propellers were simulated over a range of velocity between 10 m/s and 65 m/s.

3. Results and discussion

3.1. Inverse design integration validation

In order to validate the inverse design implementation in JBLADE, the light aircraft propeller presented by Adkins and Liebeck [20] was obtained using the implemented method. The required data for propeller inverse design are described in Table 5 and the resulting geometry is presented in Fig. 10.

Table 5
Input data for propeller inverse design.

Designation		Units
Power	52	kW
Rotation speed	2400	rpm
Hub diameter	1	ft
Tip diameter	5.75	ft
Aircraft velocity	49	m/s
Lift coefficient	0.7	
No. of blades	2	

Observing Fig. 10 is possible to conclude that JBLADE is in good agreement with original implementation done by Adkins and Liebeck [20]. The implementation was checked also against QMIL [42] since it uses a different approach for introducing the airfoil characteristics. The results have shown that similar geometries are obtained for the given propeller design point.

3.2. Propeller performance comparison

The performance of the propellers is presented in Fig. 11 in function of the advance ratio. On the left, Fig. 11(a) presents the thrust coefficient versus advance ratio, Fig. 11(b) the power coefficient, Fig. 11(c) presents the propeller efficiency.

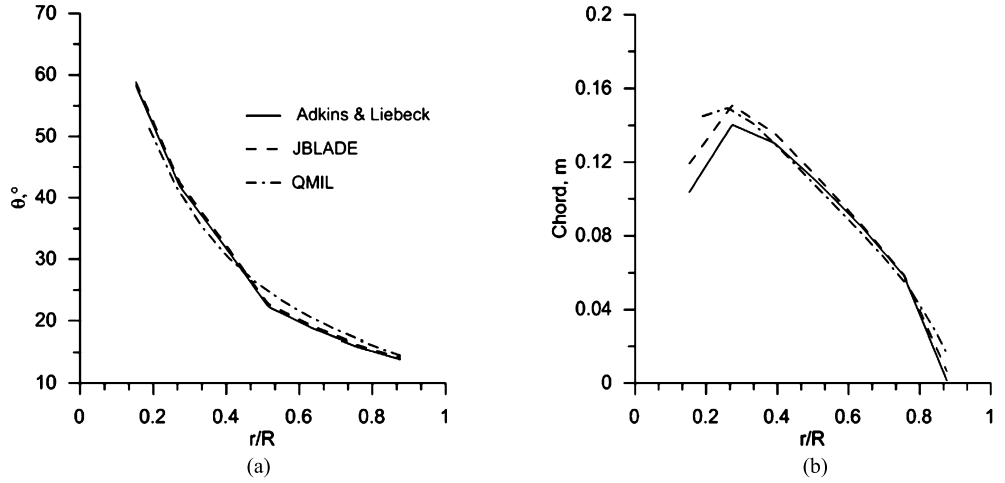

(a) (b)

Fig. 10. Comparison between data predicted by JBLADE [26,28] and QMIL [38] and Adkins and Liebeck [18] for the inverse design methodology validation. (a) Blade twist angle, (b) chord distribution.

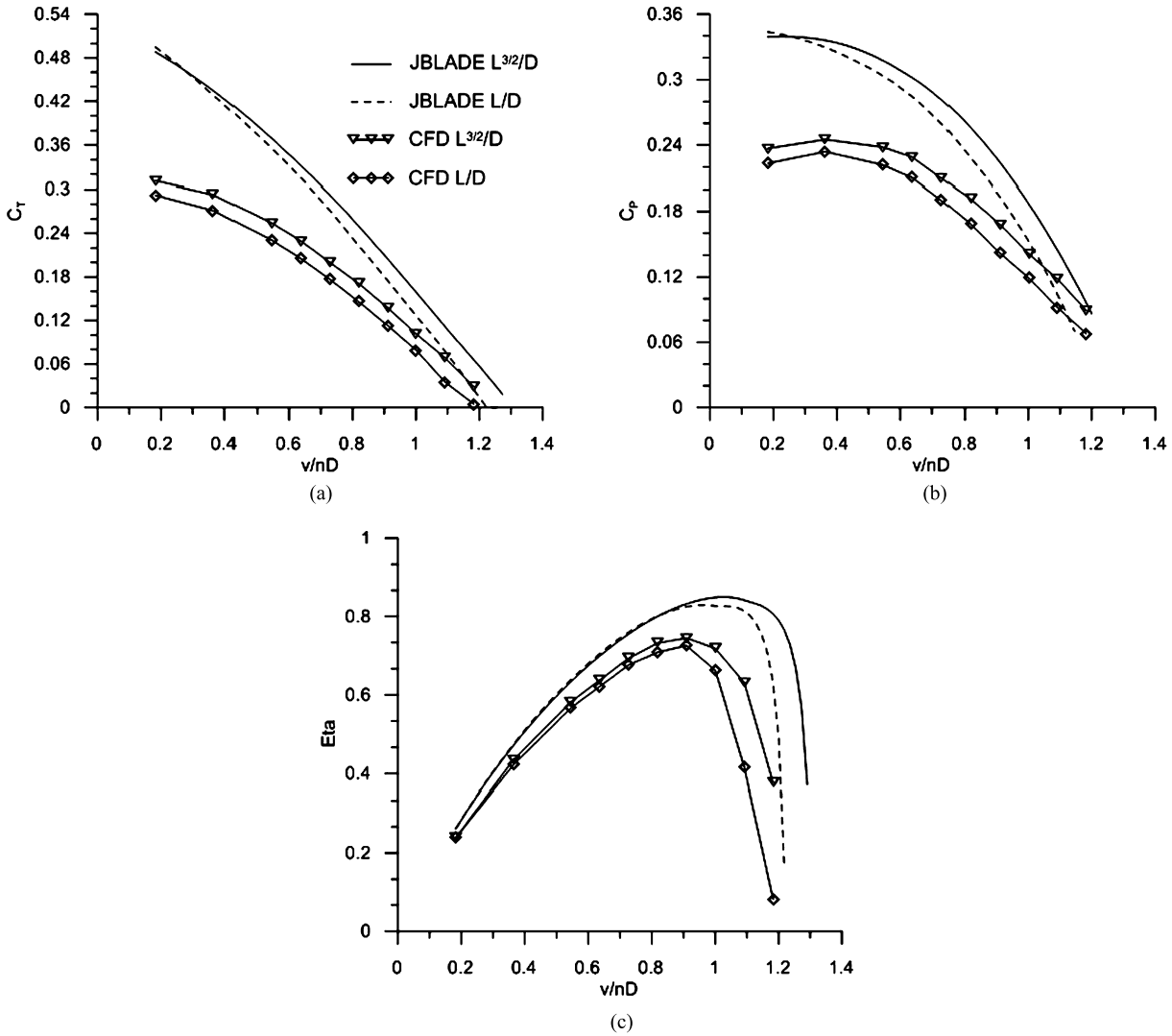

(a) (b) (c)

Fig. 11. Comparison between data predicted by JBLADE and CFD for the optimized propeller: (a) thrust coefficient, (b) power coefficient, (c) propeller efficiency.

Since there is no experimental data, the JBLADE results were compared with the CFD simulations. Observing Fig. 11 it is possible to conclude that JBLADE is in fair agreement with CFD calculations. JBLADE predicts a slightly bigger thrust coefficient than CFD in the higher advance ratio region. The results also show that the power coefficient is over estimated by JBLADE at low advance ratios when compared with CFD simulations. Due to the small differences presented in thrust and power coefficient, the propeller

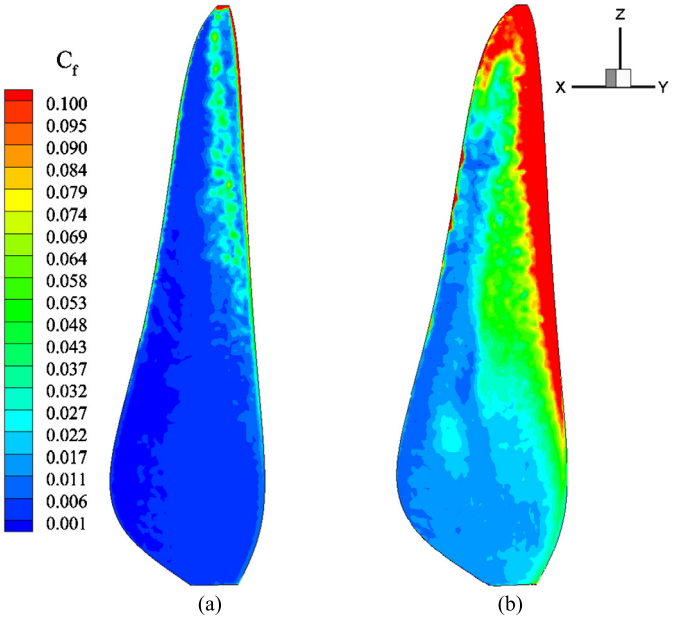

Fig. 12. Comparison of skin friction coefficient distribution on upper surfaces for $V = 30$ m/s and 550 rpm. (a) $L^{3/2}/D$ propeller, (b) L/D propeller.

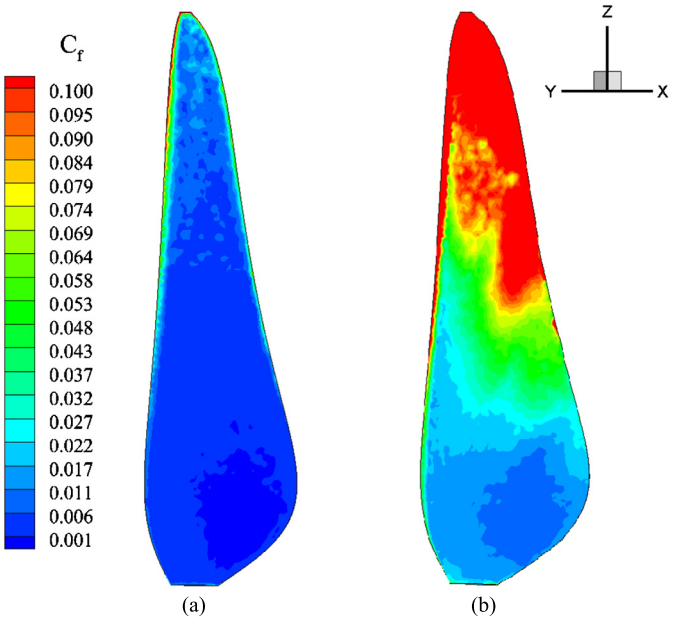

Fig. 13. Comparison of skin friction coefficient distribution on lower surfaces for $V = 30$ m/s and 550 rpm. (a) $L^{3/2}/D$ propeller, (b) L/D propeller.

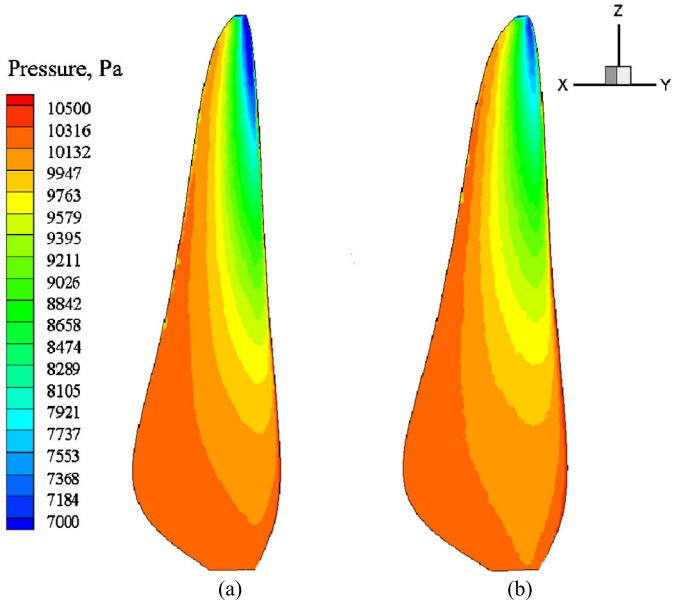

Fig. 14. Comparison of pressure distribution on upper surfaces for $V = 30$ m/s and 550 rpm. (a) $L^{3/2}/D$ propeller, (b) L/D propeller.

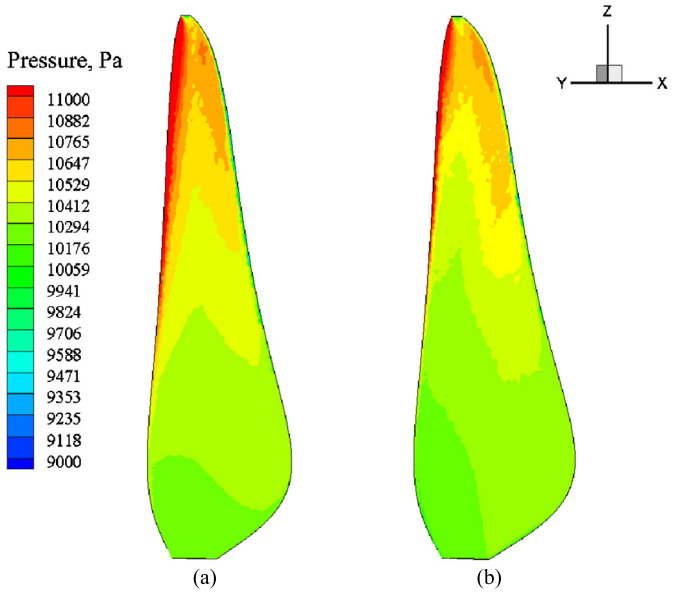

Fig. 15. Comparison of pressure distribution on lower surfaces for $V = 30$ m/s and 550 rpm. (a) $L^{3/2}/D$ propeller, (b) L/D propeller.

efficiency is slightly under predicted by JBLADE in the low advance ratio regions. The advance ratio for the maximum efficiency closely matches the CFD values but the maximum efficiency is estimated to be 10% higher than the CFD simulations values. This is related to the JBLADE's over prediction of the thrust coefficient at high advance ratios. Besides comparing JBLADE results with the CFD simulations, Fig. 11 also shows that JBLADE correctly predicts the difference between the two different design methodologies. This difference also appeared in CFD simulations and it is possible to conclude that JBLADE can be used to produce different propeller geometries and select the propeller with better performance.

In order to understand the influence of the different design concepts on the performance of the propellers, the skin friction on the blades is compared in Figs. 12 and 13. These figures clearly show that the skin friction coefficient of the blade designed using the concept of best L/D is higher than the skin friction coefficient on the blade designed using the airfoil's best $L^{3/2}/D$. This means that there is a larger viscous loss on the L/D blade's surface, which is not beneficial for the performance of the blade, since the input power will be partly used to overcome the extra drag caused by the blade shape. Most of these losses are occurring near the leading edge of the airfoil and mostly in the tip region of the blade.

Another parameter that could be used for analyzing the blade design is the pressure distribution on the blades surfaces (see Figs. 14 and 15). The thrust is originated mostly from pressures forces, which means that the larger the difference of pressure between the sides of the blade, the greater the thrust generation capability of the blade in the same operating condition.

When the blade is rotating, the upper surface of the blade presents lower pressure and the lower surface of the blade has

higher pressure. The biggest difference of pressure distributions appears on the blade tip while at the blade's root the difference is small. The comparison of the blades reveals that the $L^{3/2}/D$ propeller provides higher pressure differences all over the blade radius, which, together with lower friction along the surfaces, means higher thrust.

4. Conclusions

This paper reports the work conducted to design and analyze two different propellers for application on MAAT high altitude cruiser airship. The propellers were designed to propel the cruiser at a steady-level flight of 16 000 m above sea level. A convenient airfoil was selected and a new airfoil was developed. Its aerodynamic performance was computed with XFOIL. The inverse design methodology applied to the selected operating point produced the propeller geometry for minimum induced losses according to two different design concepts. The propeller designed with the concept of maximum $L^{3/2}/D$ generates bigger pressure differences between upper and lower surfaces with less friction which mean more thrust than the blade designed with the concept of maximum L/D.

Conflict of interest statement

The authors declare that there is no conflict of interests regarding the publication of this article.

Acknowledgements

The present work was performed as part of Project MAAT (Ref. No. 285602) supported by European Union Seventh Framework Programme. Part of the work was also supported by both C-MAST – Center for Mechanical and Aerospace Sciences and Technologies, Portuguese Foundation for Science and Technology Research Unit No. 151.

References

[1] M. Abdollahzadeh, F. Rodrigues, J.C. Páscoa, P.J. Oliveira, Numerical design and analysis of a multi-DBD actuator configuration for the experimental testing of ACHEON nozzle model, Aerosp. Sci. Technol. 41 (2015) 273–295.
[2] M. Abdollahzadeh, J.C. Páscoa, P.J. Oliveira, Modified split-potential model for modeling the effect of DBD plasma actuators in high altitude flow control, Curr. Appl. Phys. 14 (2014) 1160–1170.
[3] Z. Zheng, W. Huo, Z. Wu, Autonomous airship path following control: theory and experiments, Control Eng. Pract. 21 (Jun. 2013) 769–788.
[4] Q. Wang, J. Chen, G. Fu, D. Duan, An approach for shape optimization of stratosphere airships based on multidisciplinary design optimization, J. Zhejiang Univ. Sci. A 10 (2009) 1609–1616.
[5] E.H. Van Eaton, Airships and the Modern Military, Carlisle Barracks, 1991.
[6] L. Liao, I. Pasternak, A review of airship structural research and development, Prog. Aerosp. Sci. 45 (May 2009) 83–96.
[7] J. Morgado, M.Â.R. Silvestre, J.C. Páscoa, Parametric study of a high altitude airship according to the multi-body concept for advanced airship transport – MAAT, in: IV Conferência Nacional em Mecânica dos Fluidos, Termodinâmica e Energia, Lisbon, 2012.
[8] Y.-G. Lee, D.-M. Kim, C.-H. Yeom, Development of Korean high altitude platform systems, Int. J. Wirel. Inf. Netw. 13 (Dec. 2005) 31–42.
[9] M.S. Smith, E.L. Rainwater, Applications of scientific ballooning technology to high altitude airships, in: AIAA's 3rd Annual Aviation Technology, Integration, and Operations Technical Forum, Denver, 1971, pp. 1–8.
[10] A. Dumas, MAAT Project – Description of Work, Reggio nell'Emilia, 2011.
[11] A. Dumas, M. Trancossi, M. Madonia, I. Giuliani, Multibody advanced airship for transport, SAE Technical Paper 2011-01-2786, 2011.
[12] G. Ilieva, J. Páscoa, A. Dumas, M. Trancossi, MAAT – Promising innovative design and green propulsive concept for future airship's transport, Aerosp. Sci. Technol. 35 (2014) 1–14.
[13] A. Betz, L. Prandtl, Schraubenpropeller mit Geringstem Energieverlust, Gött. Nachr. (1919) 193–217.
[14] S. Goldstein, On the vortex theory of screw propellers, Proc. R. Soc. A, Math. Phys. Eng. Sci. 123 (Apr. 1929) 440–465.
[15] H. Glauert, Airplane propellers, in: W.F. Durand (Ed.), Aerodynamic Theory, Berlin, 1935.
[16] D. Biermann, Compromises in propeller design, J. Aeronaut. Sci. 3 (Feb. 1936) 142–144.
[17] T. Theodorsen, Theory of Propellers, McGraw–Hill Book Company, New York, 1948.
[18] E.E. Larrabee, Practical design of minimum induced loss propellers, SAE Technical Paper 790585, 1979.
[19] H.S. Ribner, S.P. Foster, Ideal efficiency of propellers – Theodorsen revisited, J. Aircr. 27 (Sep. 1990) 810–819.
[20] C.N. Adkins, R.H. Liebeck, Design of optimum propellers, J. Propuls. Power 10 (Sep. 1994) 676–682.
[21] G-520 Egrett – the Perfect Platform for High Altitude Reconnaissance and Surveillance, Grob Company, 1991.
[22] Egrett II Brochure, E-Systems GreenVille Division, 1991.
[23] A. Colozza, High altitude propeller design and analysis overview, Technical Report, Federal Data Systems, Cleveland, 1998.
[24] J.S. Monk, A propeller design and analysis capability evaluation for high altitude application, MSc Thesis, University of Witwatersrand, Johannesburg, 2010.
[25] NASA Facts – Perseus B, Dryden Flight Research Center, National Aeronautics and Space Administration, Edwards, 1999.
[26] D. Schawe, C. Rohardt, G. Wichmann, Aerodynamic design assessment of Strato 2C and its potential for unmanned high altitude airborne platforms, Aerosp. Sci. Technol. 6 (2002) 43–51.
[27] P.W. Merlin, Crash Course – Lessons Learned from Accidents Involving Remotely Piloted and Autonomous Aircraft, Monographs in Aerospace History, vol. 44, National Aeronautics and Space Administration, 2013.
[28] M.A.R. Silvestre, J.P. Morgado, J.C. Pascoa, JBLADE: a propeller design and analysis code, in: 2013 International Powered Lift Conference, Los Angeles, American Institute of Aeronautics and Astronautics, 2013.
[29] J.P. Morgado, M.A.R. Silvestre, J.C. Pascoa, Full range airfoil polars for propeller blade element momentum analysis, in: 2013 International Powered Lift Conference, Los Angeles, American Institute of Aeronautics and Astronautics, 2013.
[30] J.P. Morgado, M.A.R. Silvestre, J.C. Pascoa, Validation of new formulations for propeller design, J. Propuls. Power 31 (2014) 467–477, http://dx.doi.org/10.2514/1.B35240.
[31] J.P. Morgado, M.A.R. Silvestre, J.C. Pascoa, A comparison of post-stall models extended for propeller performance prediction, Aircr. Eng. Aerosp. Technol. (2015), http://dx.doi.org/10.1108/AEAT-07-2014-0119.R1.
[32] M.A.R. Silvestre, J. Morgado, P. Alves, P. Santos, P. Gamboa, J.C. Páscoa, Propeller performance measurements at low Reynolds numbers, Int. J. Mech. (ISSN 1998-4448) 9 (2015) 154–166.
[33] Digia, Qt Project, http://qt-project.org/ [cited: 10 July 2014].
[34] D. Marten, J. Wendler, G. Pechlivanoglou, C.N. Nayeri, C.O. Paschereit, QBLADE: an open source tool for design and simulation of horizontal and vertical axis wind turbines, Int. J. Emerg. Technol. Adv. Eng. 3 (2013) 264–269.
[35] D. Marten, J. Wendler, QBlade Guidelines v0.6, Berlin, 2013.
[36] A. Deperrois, Analysis of foils and wings operating at low Reynolds numbers – guidelines for XFLR5 v6.03, 2011.
[37] M. Drela, XFOIL – an analysis and design system for low Reynolds number airfoils, in: Proceedings of Low Reynolds Number Aerodynamics, Berlin, in: Lecture Notes in Engineering, vol. 54, 1989, pp. 1–12.
[38] U.S. Standard Atmosphere URL: http://ccmc.gsfc.nasa.gov/modelweb/atmos/us_standard.html, Washington D.C. [cited 25 September 2014].
[39] P.V. Gamboa, M.A.R. Silvestre, Airfoil optimization with transition curve as objective function, in: VI International Conference on Adaptive Modeling and Simulation ADMOS 2013, Lisbon, 2013.
[40] L.D. Koch, Design and performance calculations of a propeller for very high altitude flight, NASA/TM 1998-206637, Lewis Research Center, Cleveland, 1998.
[41] F.R. Menter, Two-equation eddy-viscosity turbulence models for engineering applications, AIAA J. 32 (Aug. 1994) 1598–1605.
[42] M. Drela, QPROP formulation, 2006.